

U-Motion: Learned Point Cloud Video Compression with U-Structured Motion Estimation

Tingyu Fan¹ Yueyu Hu¹ Yao Wang¹

¹Tandon School of Engineering, New York University

{tf2387, yyhu, yaowang}@nyu.edu

Abstract

Point cloud video (PCV) is a versatile 3D representation of dynamic scenes with many emerging applications. This paper introduces U-Motion, a learning-based compression scheme for both PCV geometry and attributes. We propose a U-Structured multiscale inter-frame prediction framework, U-Inter, which performs layer-wise explicit motion estimation and compensation (ME/MC) at different scales with varying levels of detail. It integrates both higher and lower-scale motion features, in addition to the information of current and previous frames, to enable accurate motion estimation at the current scale. In addition, we design a cascaded spatial predictive coding module to capture the inter-scale spatial redundancy remaining after U-Inter prediction. We further propose an effective context detach and restore scheme to reduce spatial-temporal redundancy in the motion and latent bit-streams and improve compression performance. We conduct experiments following the MPEG Common Test Condition and demonstrate that U-Motion can achieve significant gains over MPEG G-PCC-GesTM v3.0 and recently published learning-based methods for both geometry and attribute compression.

1. Introduction

Point cloud video is a versatile 3D representation with broad applications, including immersive volumetric video streaming, autonomous driving, and augmented reality [14, 24]. Due to the high data volume, it is essential to compress point cloud videos efficiently for data storage and transmission. This demand leads to the successful standardization of MPEG PCC (including G-PCC [23] and V-PCC [12]). Beyond these standards, numerous learning-based methods [25, 29, 34] have been proposed for compression of either static or dynamic point clouds, either for geometry (locations of points) or attributes (colors or other properties associated with points).

One essential element in point cloud video compression

is inter-frame coding, which exploits the temporal redundancy between consecutive frames. This is typically accomplished through motion estimation and compensation. However, compared with 2D videos on a regular 2D grid, the points in a PCV are irregularly spread over a small fraction of the 3D space, making the design of motion estimation and compensation approaches for PCV significantly more challenging. Moreover, to ensure superior rate-distortion performance, we need to incorporate efficient context-based coding schemes to compress the estimated motion fields as well as features for recovering the geometry or attributes. Furthermore, it is desirable to develop a codec framework that can be used for both the geometry and attributes, to save hardware design resources for future chip tape-outs. .

To address the inter-coding problem, standard approaches either project the point cloud to a 2D video and use an existing video codec for motion estimation and compensation (*i.e.* V-PCC [12]), or conduct cube-level motion compensation with a neighbor search strategy (*i.e.* G-PCC [23]). Meanwhile, some learned dynamic point cloud compression methods [30–32] have been proposed to leverage sparse convolution techniques [5] to exploit temporal correlation, known as *temporal convolution*. Specifically, the state-of-the-art scheme Unicorn [31, 32] incorporates the spatial-temporal *target convolution* to predict the current frame from the reference frame. However, these techniques limit the potential underlying motion patterns to be within the expressibility of a set of learned convolutional kernels, without the correct localization for temporal context mining offered by explicit motion estimation. This leads to suboptimal inter prediction.

To tackle the challenge of motion estimation in point cloud videos, we propose a novel unified point cloud compression scheme, named *U-Motion*, which incorporates an U-Structured inter prediction module, named *U-Inter*, to estimate and compensate motion at different scales. The U-Inter structure, akin to the popular U-Net, through the use of both top-down, bottom-up and skip connections, leverages the motion information at both upper and lower scales to in-

form motion estimation at a current scale. We also propose novel network structures for *context detach* and *context restore* for compressing motion and frame features, using the coarser motion as the context for coding the current motion, and using both inter-context (motion-compensated from the reference frame) and intra-context (upsampled from lower scale) for coding the frame features.

We evaluate our method following the MPEG Common Test Conditions (CTC)’s specification [1] for data splitting, in both geometry and color coding. The experimental results show that U-Motion outperforms the learning-based state-of-the-art Unicorn [32], as well as the rule-based MPEG standard G-PCC-GesTM-v3.0 [6] by a large margin in terms of rate-distortion (R-D) trade-off. We conduct ablation studies to validate the effectiveness of each component in our proposed U-Motion codec, and show that the proposed method is robust to different types of human point clouds and motion patterns. Our contributions can be summarized as follows:

- We propose a novel unified PCV compression scheme, named U-Motion, which incorporates a hierarchical motion estimation module using a U-Net like structure. We demonstrate the importance of both top-down and bottom-up motion calculations as well as skip connections for accurate motion estimation and efficient motion coding under rate constraint. The framework can be used for both geometry and attribute coding.
- We compress the motion feature by *contextually detaching* the estimated motion at a lower layer, and conduct a 2-stage temporal-and-spatial *context detach* to compress the attribute feature.
- We evaluate our proposed U-Motion codec following the MPEG CTC’s data splitting, for both geometry coding and color coding, and demonstrate U-Motion’s significant performance gain against the learning-based state-of-the-art method Unicorn [32] and MPEG standard G-PCC-GesTM v3.0 [6] in terms of rate-distortion trade-off.

2. Related Work

2.1. Traditional Point Cloud Video Compression

There are two primary technical routes for traditional point cloud video compression: 3D-structure-based and video-based. 3D-structure-based methods [7, 23, 27] process original point clouds directly and leverage various block-matching algorithms to identify temporal dependencies. A notable example is the MPEG standard G-PCC-GesTM [6], which has demonstrated state-of-the-art performance among all 3D-structure-based methods. In contrast, 2D-video-based methods [12, 13, 35] reuse the existing 2D video codecs by projecting the 3D point cloud video into 2D space. Among all 2D-video-based methods, the MPEG standard V-PCC achieves state-of-the-art performance.

2.2. Learning-Based Point Cloud Video Compression

Early research on learning-based point cloud compression focuses on static point clouds [10, 11, 28, 29, 34]. Wang *et al.* [28] first propose to use sparse convolution [5] to compress voxelized point clouds, and propose a multiscale architecture, as well as a local auto-regressive architecture SOPA [29] for lossless compression. To further exploit the temporal redundancy in point cloud video, some methods adopt temporal convolution for inter prediction. Anique *et al.* [2] design a predictor for geometry compression, which compensates and compresses the current frame’s latent representation based on its reference neighbors. Wang *et al.* introduce Unicorn [31, 32], a unified architecture that integrates geometry & attributes, static & dynamic compression, using context compensation and multiscale motion compensation. The temporal compensation is obtained through sparse convolution on the voxels in the previous frame, known as target convolution. However, both Unicorn and Anique *et al.*’s method lack explicit motion estimation, leading to sub-optimal temporal prediction. On the contrary, Fan *et al.* propose D-DPCC [9] with an end-to-end learning-based motion estimation and motion compensation (ME/MC) module. Xia *et al.* [33] further propose a two-layer ME/MC architecture for coarse-to-fine motion compensation. However, the above ME/MC-based methods are developed only for point cloud video geometry. In addition, their lack of a hierarchical inter- and intra-prediction structure leads to inferior coding efficiency compared to Unicorn-Geometry.

2.3. Learning-based Video Compression

Prior to learning-based point cloud compression, there have been significant advances in learned video compression [15, 16, 18–22, 26]. DVC [22] and FVC [15] are the pioneering AI video codecs that performs ME/MC on pixel domain and feature domain, respectively. These work follow a residual-coding framework which encodes the difference between the warped decoded reference frame and the current frame. Li *et al.* propose DCVC [18], which extends the residual-coding framework to context-coding, generating temporal context priors instead of warped predictions for ME/MC. DCVC-HEM [19] further proposes a parallel checkerboard entropy model supporting variable bit-rate. DCVC-DC [20] and DCVC-FM [21] further incorporate hierarchical quality structure and inter feature modulation to alleviate the accumulation of error in the temporal context. However, due to the irregular point geometry and data diversity of point cloud sequences, learning-based video compression methods cannot be directly integrated to point cloud video compression.

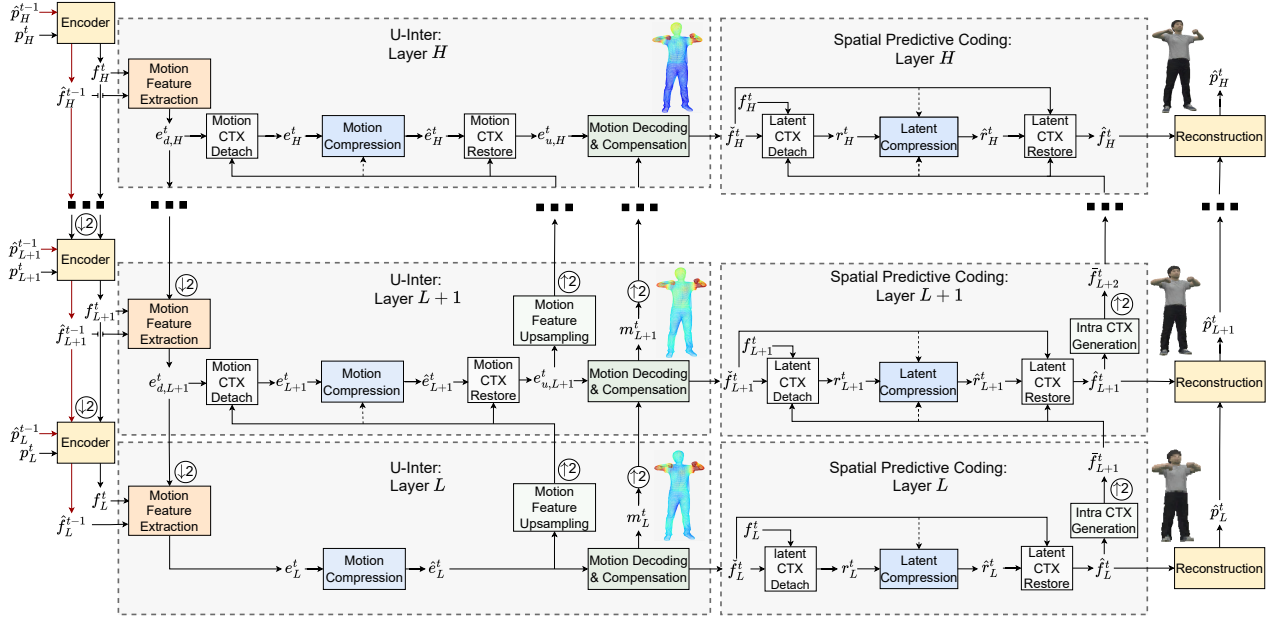


Figure 1. The overall architecture of U-Motion for color attribute coding. The dashed line denotes context connection for entropy coding. Detailed architecture of each module is provided in supplementary material.

3. Methodology

3.1. Overview of Attribute Compression

As shown in Figure 1, our method is a hierarchical architecture consisting of $(H - L + 1)$ U-Inter and Spatial Predictive Coding Layers, where the l -th layer corresponds to the l -th level of the point cloud when represented by an octree. We denote the point cloud frame (including both geometry coordinate and color attribute for each point at each octree level) at time t and layer l as p_l^t , and its reference (i.e. the decoded previous point cloud frame) as \hat{p}_l^{t-1} . p_l^t is expressed as a sparse tensor $[G(p_l^t), A(p_l^t)]$, where $G(p_l^t)$ denotes an $N \times 3$ geometry coordinate matrix and $A(p_l^t)$ denotes the corresponding $N \times 3$ attribute matrix, with N denoting the total number of points at layer l . The encoder fuses p_l^t and the upper layer's latent f_{l+1}^t to generate the latent representation f_l^t . The same encoder is also used to generate the reference frame's latent \hat{f}_l^{t-1} .

The U-Net structured U-Inter module applies both top-down and bottom-up inter prediction strategies. The top-down motion feature extraction infers the initial motion embedding $e_{d,l}^t$ between f_l^t and f_{l+1}^t , by exploiting both f_l^t and \hat{f}_{l+1}^{t-1} , as well as the higher-scale motion information $e_{d,l+1}^t$. The bottom-up inter prediction further *contextually detach* $e_{u,l-1}^t$ from $e_{d,l}^t$ to generate motion embedding e_l^t . Essentially, it removes the redundancy of $e_{d,l}^t$ conditioned on $e_{u,l-1}^t$. The motion compression module compresses and decompresses e_l^t into \hat{e}_l^t , which is then *contextually restored*

(Section 3.4) into $e_{u,l}^t$ with $e_{u,l-1}^t$ as context. The motion decoding module decodes the motion field m_l^t from $e_{u,l}^t$ and the lower layer motion m_{l-1}^t . Finally, the network performs motion compensation to generate inter context \hat{f}_l^t with m_l^t by warping and interpolation.

The Spatial Predictive Coding module further reduces the layer-wise spatial redundancy by generating an intra context \hat{f}_l^t based on the already decoded lower layer's latent \hat{f}_{l-1}^t . The inter context \hat{f}_l^t and intra context \hat{f}_l^t are then *contextually detached* from f_l^t to generate residual r_l^t . The latent compression module compresses and decompresses r_l^t into \hat{r}_l^t , which is then combined with the context \hat{f}_l^t and \hat{f}_{l-1}^t to *contextually restore* the decoded latent \hat{f}_l^t . The reconstruction module takes \hat{f}_l^t and the previous layer's latent \hat{p}_{l-1}^t to recover the color attributes in \hat{p}_l^t .

3.2. Hierarchical Attribute Encoding and Reconstruction

Latent Feature Encoder. The encoder maps the current layer p_l^t and the latent from the upper layer f_{l+1}^t into the latent representation for the current layer f_l^t . The same encoder is used to map \hat{p}_l^{t-1} and \hat{f}_{l+1}^{t-1} into \hat{f}_l^{t-1} . In contrast to Unicorn which blocks the latent from flowing between layers, our encoder fuses the higher layer's latent f_{l+1}^t , in the hope that the lower layer's latent representation encapsulate important information of the higher layers. The convolution indicated in this module refers to sparse convolution, as with all other modules of the entire network.

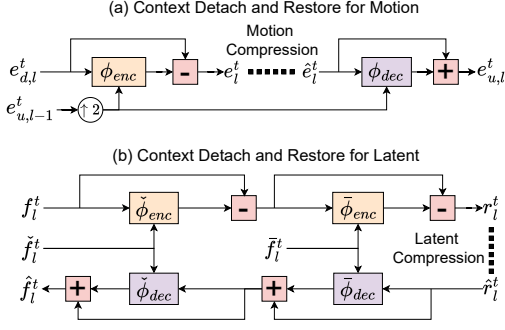


Figure 2. The network architecture for context detach and restore.

Attribute Reconstruction. The reconstruction module recovers the colors in the l -th scale point cloud \hat{p}_l^t based on the reconstructed latent \hat{f}_l^t and lower scale’s reconstruction \hat{p}_{l-1}^t . For attribute compression with geometry coordinates known, the network estimates a residual attribute Δp_l^t every layer based on the concatenation of upsampled \hat{p}_{l-1}^t and \hat{f}_l^t . The reconstruction is the sum of Δp_l^t and the upsampled \hat{p}_{l-1}^t . The upsamle of color is realized by trans-pooling.

3.3. U-Inter for ME/MC

U-Structured Inter Prediction. As shown in Figure 1, our U-Inter Prediction follows a U-Net structure, consisting of top-down and bottom-up connections between scales. At an intermediate scale (e.g. $l = L + 1$ in the figure), the motion field m_l^t is generated using both the current latent f_l^t and reference latent \hat{f}_l^t , as well as the upper-scale motion embedding $e_{d,l+1}^t$, and the lower-scale motion embedding $e_{u,l-1}^t$ and motion flow m_{l-1}^t .

Specifically, the motion feature extraction module takes the concatenation [9] of f_l^t and \hat{f}_l^t , as well as the upper-scale flow embedding $e_{d,l+1}^t$ (down-sampled to the current scale using a stride 2 convolution) as input and generates the initial motion embedding $e_{d,l}^t$ of the current layer. The top-down connection to $e_{d,l+1}^t$ enables $e_{d,l}^t$ to inherit the motion features extracted from the upper scale. However, compressing $e_{d,l}^t$ directly is suboptimal because 1) $e_{d,l}^t$ may be similar across layers; and 2) $e_{d,l}^t$ has a limited receptive field due to the lack of lower-scale information. Therefore, the bottom-up inter prediction *contextually detaches* the redundancy in $e_{d,l}^t$ that is predictable from the already decoded lower-scale $e_{u,l-1}^t$. The output after detaching, i.e. the motion embedding e_l^t is compressed and decompressed into \hat{e}_l^t . \hat{e}_l^t is then *contextually restored* into $e_{u,l}^t$ and fused with lower-scale motion information using lower-scale motion $e_{u,l-1}^t$ as context. Finally, $e_{u,l}^t$ and the estimated motion from the lower layer m_{l-1}^t (after upsampling) are input to the motion decoder to generate the estimated motion m_l^t .

Prior approaches for motion estimation often adopt a

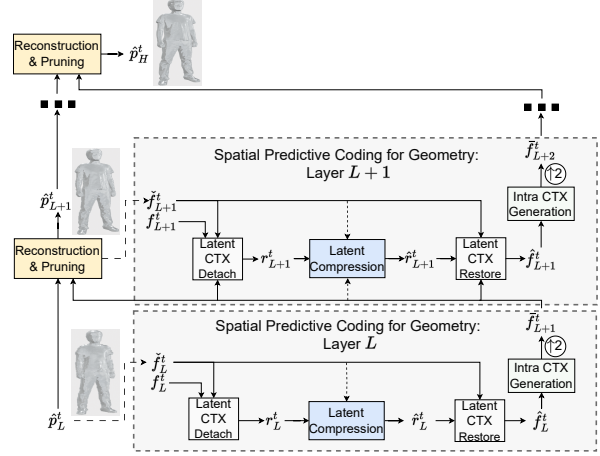


Figure 3. The architecture of Spatial Predictive Coding layer for Geometry. The dashed line denotes context connection. The long dashed line denotes the action of assigning the decoded geometry coordinate \hat{p}_l^t to U-Inter to get \hat{f}_l^t .

coarse-to-fine approach, starting with estimating the motion from the lowest scale, and then progressively determining the residual motion in each upper scale. We have observed, though, the lower scale point clouds may lack details that are necessary for estimating the motion correctly. When the top-down links in the U-Inter structure were removed, the network often yield completely zero motions, in part due to the rate constraint. The top-down connection to $e_{d,l+1}^t$ and the bottom-up connection to $e_{u,l-1}^t$ and m_{l-1}^t , through multiple scales, enable the proposed U-Inter architecture to estimate large motion effectively, by inheriting the details of upper layers for lower layer motion estimation.

Motion Decoding and Compensation. We extend the single-scale motion compensation in prior works to multi-scale to leverage the details at higher layers. To get the l -th scale motion for compensation, the motion decoding module decodes a residual motion flow Δm_l^t from both motion feature $e_{u,l}^t$ and upsampled m_{l-1}^t , which is then added to the upsampled m_{l-1}^t to generate the fine motion m_l^t . For each point with coordinate s in f_l^t , its warped position $\tilde{s} = s + m_{l,s}^t$ is likely to be invalid in \hat{f}_l^{t-1} . Therefore, we adopt the 3D Adaptive Weighted Interpolation (3DAWI) algorithm [9] to generate the inter context \hat{f}_l^{t-1} ,

$$\hat{f}_{l,s}^t = \frac{\sum_{v \in \vartheta(\tilde{s})} d_v^{-1} \cdot \hat{f}_{l,v}^{t-1}}{\max \left\{ \sum_{v \in \vartheta(\tilde{s})} d_v^{-1}, \alpha \right\}}, \quad (1)$$

where $\vartheta(\tilde{s})$ denotes the K -nearest neighbors of \tilde{s} in \hat{f}_l^{t-1} , d_v is the distance between \tilde{s} and v , α is a penalty parameter to decrease the weights of the points too far from \tilde{s} . Different from 3DAWI, We make α a learnable parameter for more

Table 1. Attribute compression BD-Rate(%) gains against G-PCC-GesTM and Unicorn. Negative values indicate bit rate reduction under same quality. **CTC-Overall** denotes the average test result on MPEG CTC sequences (The first four sequences). **Overall** denotes the average test result on all six sequences.

Sequence	G-PCC-GesTM		Unicorn	
	Y	YUV	Y	YUV
exercise_vox10	-26.41	-22.92	-30.47	-34.84
model_vox10	-40.35	-38.73	-34.78	-39.80
basketball_vox11	-3.93	-0.04	-25.05	-32.94
dancer_vox11	19.22	24.26	-2.76	-12.60
basketball_vox10	-26.17	-23.97	-31.46	-37.27
dancer_vox10	-12.36	-9.46	-17.65	-28.45
CTC-Overall	-12.86	-9.35	-22.69	-30.04
Overall	-14.99	-11.80	-23.31	-30.98

flexibility. During experiments, we set $K = 6$ and initial α to 4. α converges to 3.6 when training stops.

3.4. Spatial Predictive Coding

Layer-wise redundancy. Besides inter-frame temporal redundancy, f_i^t exhibits inter-layer spatial redundancy. Therefore, as shown in Figure 1, Spatial Predictive Coding module further removes the spatial redundancy by estimating an intra context \tilde{f}_i^t , using the already decoded lower-scale latent \hat{f}_{i-1}^t .

Context Detach and Restore. The network detaches the redundancy in f_i^t to generate residual r_i^t , then restores the reconstructed \hat{f}_i^t from the decoded residual \hat{r}_i^t using both inter context \tilde{f}_i^t and intra context \hat{f}_i^t . An intuitive way of achieving this is through mathematical addition and subtraction: Given latent f to be coded and the context f_c , generate residual $r = f - f_c$, and then recover the decompressed latent $\hat{f} = \hat{r} + f_c$, where \hat{r} indicates the quantized r . To grant the network more flexibility, Li et al. [18] propose to use an encoder and decoder to detach and restore the context, respectively:

$$r = \phi_{enc}(f|f_c; \theta_{enc}), \hat{f} = \phi_{dec}(\hat{r}|f_c; \theta_{dec}), \quad (2)$$

where ϕ_{enc} and ϕ_{dec} are two neural networks. During experiments, we find that such modules are hard to train. Compared with mathematical subtraction that directly narrows r 's distribution, the distribution of r generated by an encoder module is harder to control. Therefore, we propose to perform context detach with a residual connection:

$$r = f - \phi_{enc}(f|f_c; \theta_{enc}). \quad (3)$$

The corresponding context restore operation is:

$$\hat{f} = \hat{r} + \phi_{dec}(\hat{r}|f_c; \theta_{dec}). \quad (4)$$

Table 2. Geometry compression BD-Rate(%) gains against Unicorn and D-DPCC. **CTC-Overall** denotes the average test result on all the four sequences from MPEG CTC.

Sequence	Unicorn		D-DPCC	
	D1	D2	D1	D2
exercise_vox10	-17.95	-23.31	-35.45	-35.55
model_vox10	-18.05	-24.50	-38.95	-36.29
basketball_vox11	-28.86	-30.78	-38.42	-37.55
dancer_vox11	-26.15	-24.38	-36.69	-34.35
CTC-Overall	-22.75	-25.74	-37.37	-35.93

The proposed context detach and restore operation grants the network with equivalent flexibility as Equation 2, but also provides the network with a "shortcut" to narrow r 's distribution. Figure 2 shows the corresponding architecture of context detach and restore with residual connections. For motion embedding e_i^t , only one such module is used with context $e_{u,l-1}^t$. For latent f_i^t , a two-stage spatial-and-temporal context detach and restore module is employed to exploit the inter context \tilde{f}_i^t and intra context \hat{f}_i^t .

3.5. Entropy Coding and Variable Rate Coding

The entropy coding module encodes the input x ($x = e_i^t$ for motion compression and r_i^t for latent compression) into a bitstream. We adopt the popular learnt compression approach, which uses both hyperprior and context features to estimate the probability distribution for quantized x [3, 4]. See more detail in the supplement. For motion compression, the context $x_c = [e_{u,l-1}^t, m_{i-1}^t]$. For latent compression, $x_c = [\tilde{f}_i^t, \hat{f}_i^t]$. We adopt the global-and-local quantization scheme proposed in DCVC-FM [21], which generates the quantization stepsizes from a given rate control parameter λ . This enables a variety of bit rates with only one compression model.

3.6. Geometry Compression

Our network can also be used for point cloud video geometry compression with slight modification. For geometry, the l -th layer point cloud $p_i^t = [G(p_i^t), O(p_i^t)]$, where $O(p_i^t)$ is an all-one vector indicating the occupancy. The same encoder structure is used to generate the latent f_i^t and \hat{f}_i^{t-1} . To code f_i^t , because the actual geometry is not known yet at the decoder, we cannot generate the inter context \tilde{f}_i^t . Rather we first reconstruct \hat{p}_i^t from \hat{f}_i^t , which is generated from \hat{f}_{i-1}^t by sparse generative deconvolution with no target coordinates specified. The reconstruction is done by the APU module in Unicorn [31], which will estimate the probability that each voxel in \hat{f}_i^t is occupied. For lossy compression, the top-N voxels in \hat{f}_i^t with the highest occupancy probability will be kept to reconstruct \hat{p}_i^t ; for lossless compression, arithmetic coder will be used to code p_i^t losslessly using the

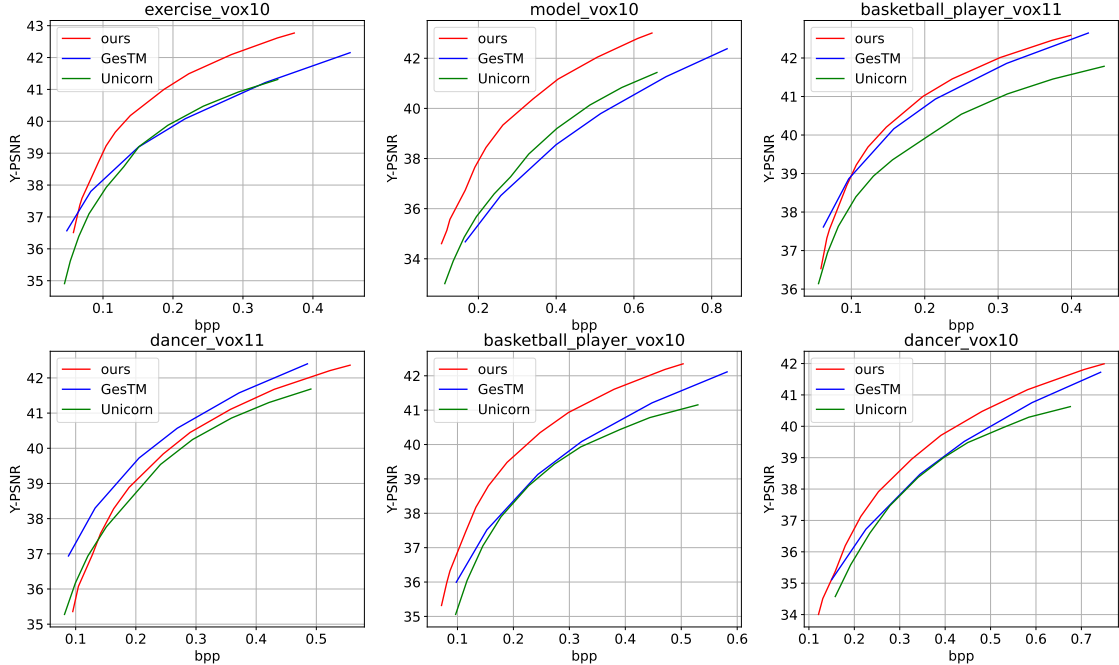


Figure 4. Y-PSNR Performance comparison on attribute (color) compression among our method, Unicorn and G-PCC-GesTM.

estimated occupancy probability (thus $\hat{p}_i^t = p_i^t$). Based on the decoded \hat{p}_i^t we can use the same U-Inter module shown in Fig. 1 to generate the temporal context \tilde{f}_i^t . Then using \tilde{f}_i^t and spatial context \tilde{f}_i^t , we code the current frame latent f_i^t using the network architecture shown in Fig. 3. In other word, for geometry, f_i^t is coded to help the reconstruction of \hat{p}_{i+1}^t instead of \hat{p}_i^t .

4. Experiments

4.1. Training and Testing Datasets

We follow the MPEG AI-3DG Common Test Condition (CTC), which specifies using the 8i Voxelized Full Bodies (8iVFB) [8] dataset for training, and the OwlII [17] dataset for testing. 8iVFB has a data precision of 10 bits and contains four sequences: *soldier*, *longdress*, *redandblack* and *loot*. OwlII contains four sequences in 11 bits precision: *basketball_player*, *dancer*, *exercise*, *model*. Following MPEG CTC’s requirement, we use 10-bit versions of *model* and *exercise* for testing provided by MPEG.

4.2. Experimental Settings

Training Details. For attribute compression, we use the layer-wise joint rate-distortion loss function:

$$L = \sum_{l=L}^H R_{r,l} + R_{m,l} + \lambda \|p_l^t - \hat{p}_l^t\|_2^2, \quad (5)$$

where $R_{r,l}$ is the bit-rate of latent at layer l and $R_{m,l}$ the bit-rate of motion. Note that p_l^t is in YUV-space. We train

only one model with $\lambda \in [256, 18000]$. λ is randomly picked from $[256, 18000]$ for each iteration. We train our model with one NVIDIA A100-SXM4-80GB, and the overall training time is 4 days. During training, we use the lossless previous frame, *i.e.* p^t as reference and only train one P-frame for each iteration. For geometry compression, the training details are in supplementary material.

Baselines. For learning-based baseline, we compare with learning-based state-of-the-art Unicorn [31, 32]. Because the code for Unicorn is not publicly available, we implemented their methods for both geometry and attribute compression. We strictly follow the setting reported in the paper and train their model also for 4 days for fairness. For attribute, the results reported in [32] were obtained by mixing the 6 sequences from 8iVFB and OwlII for training and testing on *soldier* from 8iVFB and *basketball_player* from OwlII. We train their model using 8iVFB dataset only to meet the MPEG CTC, which yields lower performance for *basketball_player* than that reported in [32] due to the data distribution difference. For geometry compression, we also compare with D-DPCC [9], and the test results were provided by the authors.

For rule-based attribute compression standards, we compare with MPEG G-PCC-GesTM-v3.0 following the settings in [32]. For geometry compression, as results shown in D-DPCC and Unicorn have demonstrated significant gain against G-PCC-GesTM and V-PCC, we only compare with learning-based methods D-DPCC and Unicorn.

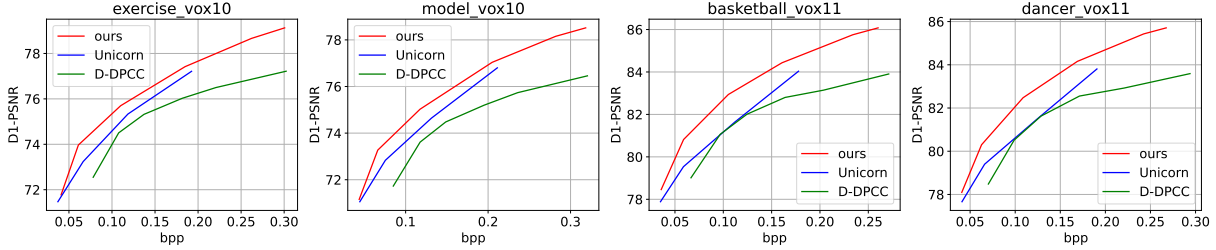


Figure 5. D1-PSNR performance comparison on lossy geometry compression among our method, Unicorn and D-DPCC

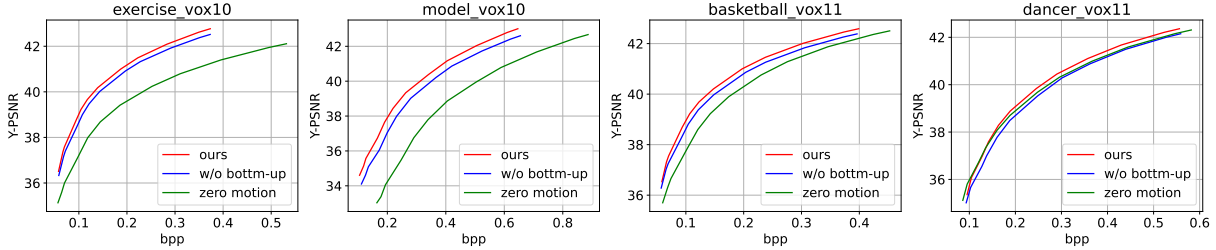


Figure 6. Ablation study on the contribution of motion flow.

Metrics. We use MPEG reference software *pc_error* to calculate distortion: D1-PSNR and D2-PSNR for geometry; Y-PSNR and YUV-PSNR (See supplementary material) for attribute. We also compare the BD-rate of each R-D curve.

4.3. Results

Attribute Compression. The R-D curves of attribute compression performance comparison is shown in Figure 4, with the corresponding BD-Rate detailed in Table 1. Please refer to the supplementary material for R-D curves with the YUV-PSNR. we assume the point cloud geometry is losslessly coded and not factored into the bit rate consumption. In addition, to remove the influence of I-frame, we use the original point cloud as I-frame, and do not consider the bits of I-frame when determining the bit rate (for U-Motion and baselines). We test the first 32 frames in each sequence. Each P-frame p^t is coded using the reconstructed previous frame \hat{p}^{t-1} as reference except for the first P-frame. Our method achieves significant gain against G-PCC-GesTM v3.0 and Unicorn on two 10-bit MPEG sequences *exercise* and *model*. Our method does not perform as well on 11-bit sequences *basketball_player* and *dancer* as on 10-bit sequences. We attribute this to the fact that the MPEG-specified training data are all 10-bit and have relatively smaller motion than these two 11 bits sequences, leading to a significant difference between training and testing data. When compared to the 10 bit versions of these two sequences, *basketball_player_vox10* and *dancer_vox10*, our method achieve more significant gains. Figure 7 shows that U-Motion achieves better visual quality at a lower bit-rate compared to other methods (sequence *model_vox10*).

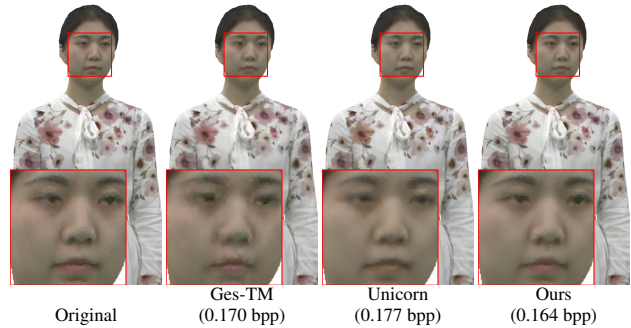


Figure 7. Rendering results from reconstructed point clouds.

Geometry Compression. Figure 5 shows the lossy geometry compression performance comparison in terms of D1-PSNR. D2-PSNR R-D curve is in supplementary material. Table 2 reports both the D1-PSNR and D2-PSNR BD-rate. It's shown that our method outperforms the previous state-of-the-art method Unicorn and the first learning-based point cloud video compression method D-DPCC.

5. Ablation Study

5.1. Impact of Motion Estimation Methods

Figure 6 compares our method U-Motion with two variations, differing in motion estimation. For “zero motion”, we set the estimated motion to zero (the temporal context at each point is thus the interpolated feature of K nearest neighbors of this point in the reference frame), and deduct the motion bit rate from the overall bit rate. Despite of the removal of the bits for coding motion features, the efficiency reduction of inter context leads to significant loss

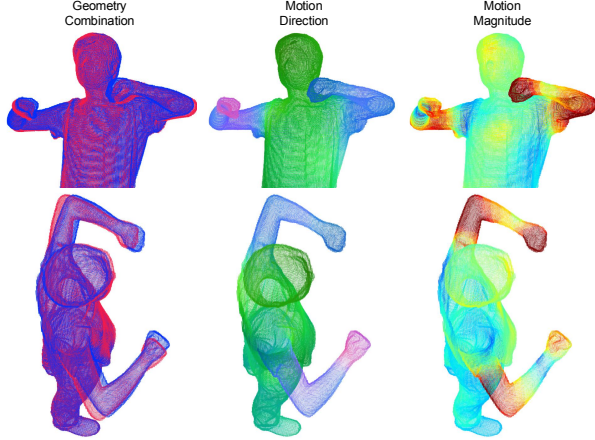


Figure 8. Visualizing motion field from two viewing angles. The point cloud in the leftmost column moves from red to blue.

in R-D performance for the two 10-bit sequences. The performance loss is less pronounced for the two 11-bit sequences, likely due to the mismatch in the bit depth and motion characteristics of these sequences from the 10 bit sequences used in the training set. These results demonstrate the unequivocal benefits of explicit motion estimation. For “w/o bottom up”, we remove the bottom-up motion context by setting $e_l^t = e_{d,l}^t$. This leads to the increase in motion bits and reduces the overall R-D performance for all sequences and rate points. To assess the importance of the top-down connection in Figure 1, we trained a network without such a connection. We found that the network converges to spending no bits for coding motion, leading to similar results as zero-motion. We attribute this to the fact that 1) the lower-scale latent contains insufficient details for accurate motion estimation; 2) the inefficiency of compressing the high-scale motion without downsampling to lower-scale leads the network to allocate all bits for coding the latent. These results together reinforce the benefit of both top-down and bottom-up connections in the proposed U-structure for motion estimation under rate constraints.

5.2. Motion Visualization

Figure 8 visualizes the motion estimated by our U-Inter module. The overlay of points of two frames on the left shows the movement between the two frames, where the hands and arms moving in opposite directions have the largest motion. This is reflected by the direction and magnitude plots of the estimated motion, demonstrating the effectiveness of the proposed U-Motion scheme.

5.3. Function of Context Detach

This section demonstrates the function of the context detach and restore. Figure 9 visualizes one variable in the latent f_l^t before context detach and the residual r_l^t after context de-

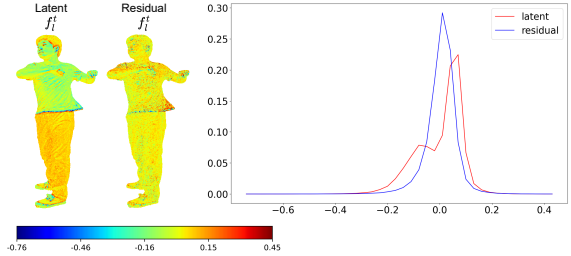


Figure 9. Visualization of latent variable f_l^t , residual r_l^t and the histogram depicting the distribution of f_l^t and r_l^t .

Table 3. Comparison of Computation Time

Method	Ours		Unicorn		Ges-TM	
precision	10	11	10	11	10	11
enc time (s)	1.21	6.31	0.98	3.42	10.11	27.28
dec time (s)	0.82	4.75	0.67	2.56	7.18	33.81

tach. Compared with r_l^t , each region of f_l^t shows relatively similar color distribution, indicating strong spatial dependencies. After contextual detachment, r_l^t looks more like noise, indicating that most of the spatial redundancy is removed. We further show the distribution of one variable of f_l^t and r_l^t . We can observe that f_l^t 's distribution is narrowed by contextual detachment.

5.4. Complexity

Table 3 compares the attribute compression complexity for our model, Unicorn and G-PCC-GesTM in terms of encoding and decoding times. U-Motion takes more time than Unicorn (about 25% more for 10 bit point cloud, about 85% for 11 bit) mainly due to the need for K-NN search for motion compensation. We use pytorch3d's implementation of K-NN with $O(N^2)$ complexity, leading to large amount of computation on point clouds with 0.7 – 3 million points. However, the K-NN complexity can be greatly reduced if local K-NN applied. We compare the complexity of geometry compression in supplementary material.

6. Conclusion

We present U-Motion, a unified PCV codec achieving state-of-the-art performance for both attributes and geometry. The key innovation is to employ U-Structured motion estimation to capture motions of different scales under rate constraints. We also propose a novel context detach and restore module for efficient coding of motion and latent features. We show U-Motion's applicability to both geometry and attribute, achieving significant gains over state-of-the-art methods. Our future work includes multi-frame training to alleviate error-propagation, reducing K-NN complexity for motion compensation and pretraining for U-Inter.

U-Motion: Learned Point Cloud Video Compression with U-Structured Motion Estimation

Supplementary Material

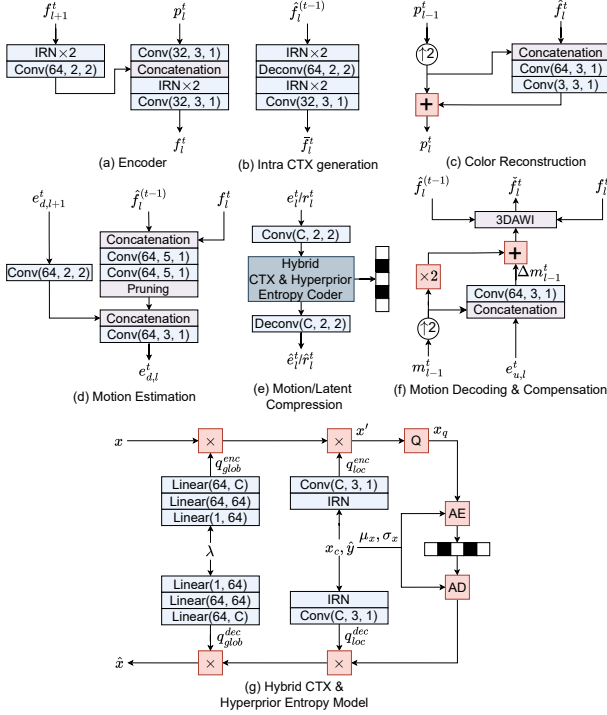


Figure 10. Detailed architectures of each module. $\text{Conv}(C, K, S)$ denotes a convolution layer with C output channels, $K \times K \times K$ convolution kernel, and $S \times S \times S$ stride. Similar notations is used for $\text{Deconv}(C, K, S)$, but S indicates the upsampling factor. IRN denotes the Inception ResNet Block [28]. $\text{Linear}(I, O)$ denotes a linear layer with I input channels and O output channels. In (e) and (g), C denotes the number of channels of the variable to be entropy coded. $C = 32$ for latent compression and $C = 24$ for motion compression.

1. Detailed Architecture of each module

This section shows the detailed architecture of each module mentioned in Section 3.

1.1. Motion Estimation

Note that the concatenation operation in Figure 10 (d) concatenates \hat{f}_i^{t-1} and f_i^t , which in general have different sets of geometry coordinates. The concatenation operation of features over two point clouds p^i and p^j is defined over the union of points in p^i and p^j as:

$$f_{cat,u} = \begin{cases} f_u^i \oplus f_u^j, & u \in p^i \cap p^j \\ f_u^i \oplus \mathbf{0}, & u \in p^i, u \notin p^j \\ \mathbf{0} \oplus f_u^j, & u \in p^j, u \notin p^i \end{cases} \quad (6)$$

where u is a coordinate in the union of the geometry coordinates of f^i and f^j , \oplus denotes the array concatenation. Note that the concatenation of \hat{f}_i^{t-1} and f_i^t covers more geometry coordinates than f_i^t . The pruning operation after convolution keeps the geometry points in f_i^t only.

1.2. Motion/Latent Compression

The architecture of Motion/Residual Compression is shown in Figure 10 (e). The input e_i^t/r_i^t is first downsampled by a stride-two convolution layer, compressed/decompressed by the *Hybrid CTX & Hyperprior Entropy Coder* and upsampled by a stride-two deconvolution layer to the corresponding reconstruction \hat{e}_i^t/\hat{r}_i^t . $C = 32$ for latent compression and $C = 24$ for motion compression. The architecture of *Hybrid CTX & Hyperprior Entropy Coder* is shown in Figure 10 (g). We adopt the global-and-local rate control [19–21] to achieve various rate points with only one model, controlled by λ . q_{glob}^{enc} and q_{glob}^{dec} are generated from the given λ to control the quantization stepsizes for different channels. q_{loc}^{enc} and q_{loc}^{dec} are generated by context x_c and hyperprior y to control local quantization steps. The quantization of x is formulated by:

$$x_{q,u} = \lfloor x_u \times (1 + q_{glob}^{enc}) \times (1 + q_{loc,u}^{enc}) \rfloor, \quad (7)$$

where u is a point in x . Rounding is replaced by adding noise during training. The dequantization is formulated by:

$$\hat{x}_u = x_{q,u} \times (1 + q_{glob}^{dec}) \times (1 + q_{loc,u}^{dec}). \quad (8)$$

We denote x_q before quantization as x' , and assume that each element of x' follows a Gaussian distribution $N(\mu, \sigma)$, where μ and σ are estimated by the context x_c . The probability of x_q can be calculated by:

$$p_{x_q}(x_q) = c_{x'}(x_q + 0.5) - c_{x'}(x_q - 0.5), \quad (9)$$

where $c_{x'}$ is the CDF of Gaussian distribution.

2. Experiments

2.1. Settings for Attribute Compression

Our U-Motion attribute compression model consists of five layers, *i.e.* five U-Inter layer and five Spatial Predictive Coding layer. We adopt the base layer strategy employed in YOGA [34], which compresses the lower-scale point cloud p_{H-3}^t with G-PCC-GesTM to provide a base for the hierarchical reconstruction. Note that for layer $l \in [L, H - 3]$, although the color is coded by GesTM, there still exists the

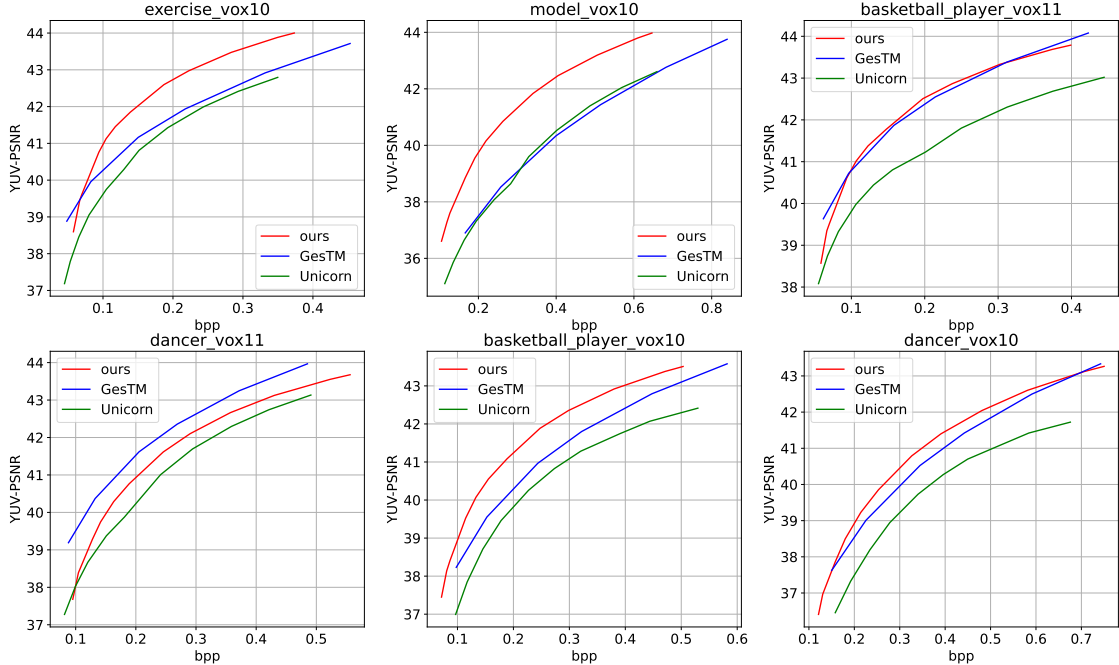


Figure 11. YUV-PSNR Performance comparison on attribute (color) compression among our method, Unicorn and G-PCC-GesTM.

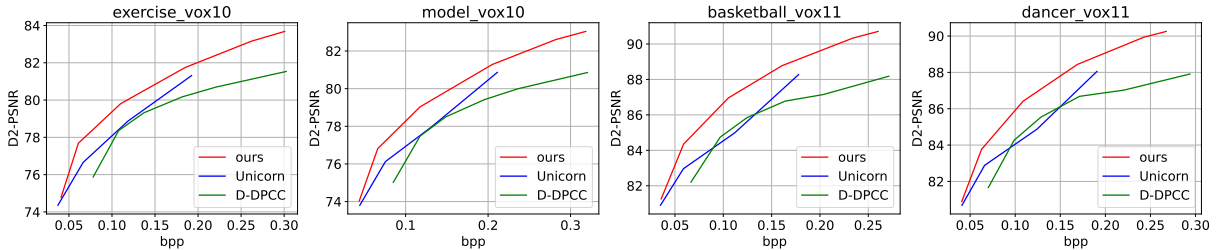


Figure 12. D2-PSNR performance comparison on lossy geometry compression among our method, Unicorn and D-DPCC

motion embedding e_l^t and latent residual r_l^t to be coded by our network for higher layers’ reconstruction. We do not losslessly compress p_l^t at layer $H - 3$ due to the excessive bit-rate consumption. Instead, we use different GesTM quantization parameters (QP) for different rate points to achieve the R-D balance of overall performance. We traverse different combinations of λ and QP on a subset of dataset and get the most R-D efficient pairs: $\lambda = [300, 460, 705, 910, 1655, 2537, 3888, 5960, 9134, 14000, 16000]$, and the corresponding $QP = [20, 20, 16, 16, 16, 16, 12, 12, 8, 8, 8]$.

2.2. Settings for Geometry Compression

As mentioned in Section 3.6, the APU module [31] supports both lossless and lossy geometry compression. For geometry, we use different combinations of lossless/lossy compression layers and different λ to realize different rate points. Given a geometry U-Motion model with $(H - L + 1)$ layers and λ as R-D factor, where $L \rightarrow M$ layers are loss-

less and $M + 1 \rightarrow H$ are lossy, the loss function \mathcal{L} during training is:

$$\mathcal{L} = \sum_{l=L}^H R_{r,l} + R_{m,l} + \lambda_l BCE(\tilde{p}_l^t, p_l^t), \quad (10)$$

where $\lambda_l = 1$ for lossless layer, $\lambda_l = \lambda$ for lossy layer, \tilde{p}_l^t is the decoded occupancy probability mentioned in Section 3.6. We train six models corresponding to the six rate points. The first three models consist of 1 lossless layer and 2 lossy layer, with $\lambda = 0.5, 1, 2$. The last three models consist of 2 lossless layers and 1 lossy layer, with $\lambda = 2, 5, 7$.

2.3. Results

YUV-PSNR for Attribute Compression. We provide the YUV R-D curve in Figure 11. Note that the MPEG reference software *pc_error* does not compute YUV-PSNR directly. Instead, we use *pc_error* to get Y-, U- and V-PSNR

Table 4. the bpp and Y-PSNR of the visualized point cloud videos.

	qp1		qp2		qp3	
	bpp	Y-PSNR	bpp	Y-PSNR	bpp	Y-PSNR
exercise_vox10	0.071	37.09	0.257	41.53	0.479	42.87
model_vox10	0.098	36.29	0.329	41.19	0.742	43.02
basketball_vox11	0.081	36.62	0.291	41.42	0.425	42.74
dancer_vox11	0.142	34.77	0.474	41.13	0.528	42.50

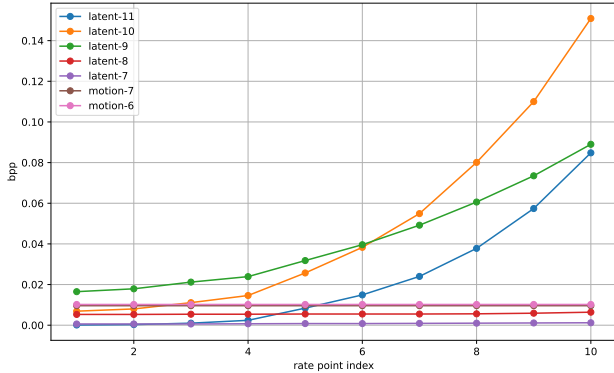


Figure 13. Rate allocation between motion and latent over different layers corresponding to different rate points for *basketball_player*, frame index 00000016.

and calculate YUV-PSNR as:

$$PSNR_{YUV} = \frac{6PSNR_Y + PSNR_U + PSNR_V}{8}. \quad (11)$$

We can observe that the performance comparison is basically consistent with Y-PSNR result.

D2-PSNR for Geometry Compression. We provide the D2 R-D curve in Figure 12. We can observe that the performance comparison is basically consistent with D1-PSNR result.

Rate Allocation. Figure 13 shows the bit-rate for coding each layer’s motion embedding e_i^t and latent residual r_i^t for one test sequence. The same trend is observed for other sequences. *latent-l* and *motion-l* denotes the bit-rate consumption of coding r_i^t and e_i^t . Note that layers not plotted have zero bits. We can observe that: 1) The bit-rate of motion information remains consistent regardless of the overall bit-rate. We attribute this to the fact that motion bit-rate only contributes to a small portion of overall bit-rate, and reducing motion bit-rate may result in the low quality of inter context \hat{f}_i^t . Therefore, the learnt network may have used the same quantization stepsizes regardless the target total rate. 2) Only the two lowest layers (Layer 6 and 7) have motion bits. We believe that this is due to the inefficiency

Table 5. Comparison of Geometry Computation Time

Method	Ours		Unicorn		D-DPCC	
precision	10	11	10	11	10	11
enc time (s)	0.64	7.42	0.45	3.15	0.67	8.75
dec time (s)	0.56	6.95	0.52	3.42	0.56	8.42

of coding residual motion in higher layers, relative to using all the bits for coding the latent. 3) The rate allocation for the latents across layers depend on the target total bit rate. At the higher rate, the higher layers take more bits (except the highest layer). At the lower rate, some intermediate layers were given more rates. Given these observations, in future improved versions of the codec, we may choose not to estimate residual motion at higher layers, and directly use the upsampled motion from lower layers for generating the inter context at higher layers. This may reduce the encoding complexity, without sacrificing the rate-quality trade-off.

Geometry Compression Complexity. For geometry compression, the complexity is related to the model architecture of each rate point. We only compare the model related to the highest rate point, *i.e.* 1 lossy and 2 lossless layers. The complexity is shown in Table 5.

Visualization of Motion Video. We visualize the point cloud motion magnitude video in folder *motion_mag*. We can observe that areas with larger movements have brighter colors.

Visualization of Reconstructed Video. We visualize the reconstructed point cloud video in folder *recon*. We pick one high bit-rate ($\lambda = 16000, QP = 8$), one medium bit-rate ($\lambda = 5960, QP = 12$) and one low bit-rate ($\lambda = 300, QP = 20$). The corresponding bpp and Y-PSNR of each sequence, each rate point is shown in Table 4.

References

- [1] Anique Akhtar and Geert Van Der Auwera. [ai-3dgc][ee5.6] summary report of ee 5.6 on dataset selection for ai-pcc call

- for proposal (cfp). *MPEG-I WG 07 MPEG 3D Graphics Coding and Haptics Coding*, m66563, 2024. 2
- [2] Anique Akhtar, Zhu Li, and Geert Van der Auwera. Inter-frame compression for dynamic point cloud geometry coding. *IEEE Transactions on Image Processing*, 2024. 2
- [3] Johannes Ballé, Valero Laparra, and Eero P Simoncelli. End-to-end optimized image compression. In *5th International Conference on Learning Representations, ICLR 2017*, 2017. 5
- [4] Johannes Ballé, David Minnen, Saurabh Singh, Sung Jin Hwang, and Nick Johnston. Variational image compression with a scale hyperprior. In *International Conference on Learning Representations*, 2018. 5
- [5] Christopher Choy, JunYoung Gwak, and Silvio Savarese. 4d spatio-temporal convnets: Minkowski convolutional neural networks. In *CVPR*, pages 3075–3084, 2019. 1, 2
- [6] WG 07 MPEG 3D Graphics Coding and Haptics Coding. G-pcc 2nd edition codec description. *MPEG-I WG 07 MPEG 3D Graphics Coding and Haptics Coding*, w23041, 2023. 2
- [7] Ricardo L de Queiroz and Philip A Chou. Motion-compensated compression of dynamic voxelized point clouds. *IEEE Transactions on Image Processing*, 26(8): 3886–3895, 2017. 2
- [8] Eugene d’Eon, Bob Harrison, Taos Myers, and Philip A Chou. 8i voxelized full bodies-a voxelized point cloud dataset. *ISO/IEC JTC1/SC29 Joint WG11/WG1 (MPEG/JPEG) input document WG11M40059/WG1M74006*, 7:8, 2017. 6
- [9] Tingyu Fan, Linyao Gao, Yiling Xu, Zhu Li, and Dong Wang. D-dpcc: Deep dynamic point cloud compression via 3d motion prediction. In *Proceedings of the Thirty-First International Joint Conference on Artificial Intelligence, IJCAI-22*, pages 898–904. International Joint Conferences on Artificial Intelligence Organization, 2022. Main Track. 2, 4, 6
- [10] Guangchi Fang, Qingyong Hu, Hanyun Wang, Yiling Xu, and Yulan Guo. 3dac: Learning attribute compression for point clouds. In *Proceedings of the IEEE/CVF Conference on Computer Vision and Pattern Recognition*, pages 14819–14828, 2022. 2
- [11] Chunyang Fu, Ge Li, Rui Song, Wei Gao, and Shan Liu. Octtattention: Octree-based large-scale contexts model for point cloud compression. In *Proceedings of the AAAI conference on artificial intelligence*, pages 625–633, 2022. 2
- [12] Danillo Graziosi, Ohji Nakagami, Shinroku Kuma, Alexandre Zaghetto, Teruhiko Suzuki, and Ali Tabatabai. An overview of ongoing point cloud compression standardization activities: Video-based (v-pcc) and geometry-based (g-pcc). *APSIPA Transactions on Signal and Information Processing*, 9:e13, 2020. 1, 2
- [13] Lanyi He, Wenjie Zhu, and Yiling Xu. Best-effort projection based attribute compression for 3d point cloud. In *2017 23rd Asia-Pacific Conference on Communications (APCC)*, pages 1–6. IEEE, 2017. 2
- [14] Yueyu Hu, Ran Gong, Qi Sun, and Yao Wang. Low latency point cloud rendering with learned splatting. In *Proceedings of the IEEE/CVF Conference on Computer Vision and Pattern Recognition*, pages 5752–5761, 2024. 1
- [15] Zhihao Hu, Guo Lu, and Dong Xu. Fvc: A new framework towards deep video compression in feature space. In *Proceedings of the IEEE/CVF Conference on Computer Vision and Pattern Recognition*, pages 1502–1511, 2021. 2
- [16] Zhihao Hu, Guo Lu, Jinyang Guo, Shan Liu, Wei Jiang, and Dong Xu. Coarse-to-fine deep video coding with hyperprior-guided mode prediction. In *Proceedings of the IEEE/CVF Conference on Computer Vision and Pattern Recognition*, pages 5921–5930, 2022. 2
- [17] Cao Keming, Xu Yi, Lu Yao, and Wen Ziyu. Owlly dynamic human mesh sequence dataset. *Document ISO/IEC JTC1/SC29/WG11 m42816*, San Diego, 2018. 6
- [18] Jiahao Li, Bin Li, and Yan Lu. Deep contextual video compression. *Advances in Neural Information Processing Systems*, 34:18114–18125, 2021. 2, 5
- [19] Jiahao Li, Bin Li, and Yan Lu. Hybrid spatial-temporal entropy modelling for neural video compression. In *Proceedings of the 30th ACM International Conference on Multimedia*, pages 1503–1511, 2022. 2, 1
- [20] Jiahao Li, Bin Li, and Yan Lu. Neural video compression with diverse contexts. In *Proceedings of the IEEE/CVF Conference on Computer Vision and Pattern Recognition*, pages 22616–22626, 2023. 2
- [21] Jiahao Li, Bin Li, and Yan Lu. Neural video compression with feature modulation. In *Proceedings of the IEEE/CVF Conference on Computer Vision and Pattern Recognition*, pages 26099–26108, 2024. 2, 5, 1
- [22] Guo Lu, Wanli Ouyang, Dong Xu, Xiaoyun Zhang, Chunlei Cai, and Zhiyong Gao. Dvc: An end-to-end deep video compression framework. In *Proceedings of the IEEE/CVF conference on computer vision and pattern recognition*, pages 11006–11015, 2019. 2
- [23] Ohji Nakagami, Sebastien Lasserre, Sugio Toshiyasu, and Marius Preda. White paper on g-pcc. In *ISO/IEC JTC 1/SC 29/AG 03 N0111*, 2023. 1, 2
- [24] Ziyu Shan, Yujie Zhang, Qi Yang, Haichen Yang, Yiling Xu, Jenq-Neng Hwang, Xiaozhong Xu, and Shan Liu. Contrastive pre-training with multi-view fusion for no-reference point cloud quality assessment. In *Proceedings of the IEEE/CVF Conference on Computer Vision and Pattern Recognition*, pages 25942–25951, 2024. 1
- [25] Xihua Sheng, Li Li, Dong Liu, Zhiwei Xiong, Zhu Li, and Feng Wu. Deep-pcac: An end-to-end deep lossy compression framework for point cloud attributes. *IEEE Transactions on Multimedia*, 24:2617–2632, 2021. 1
- [26] Xihua Sheng, Jiahao Li, Bin Li, Li Li, Dong Liu, and Yan Lu. Temporal context mining for learned video compression. *IEEE Transactions on Multimedia*, 25:7311–7322, 2022. 2
- [27] Dorina Thanou, Philip A Chou, and Pascal Frossard. Graph-based motion estimation and compensation for dynamic 3d point cloud compression. In *2015 IEEE International Conference on Image Processing (ICIP)*, pages 3235–3239. IEEE, 2015. 2
- [28] Jianqiang Wang, Dandan Ding, Zhu Li, and Zhan Ma. Multi-scale point cloud geometry compression. In *2021 Data Compression Conference (DCC)*, pages 73–82. IEEE, 2021. 2, 1

- [29] Jianqiang Wang, Dandan Ding, Zhu Li, Xiaoxing Feng, Chuntong Cao, and Zhan Ma. Sparse tensor-based multiscale representation for point cloud geometry compression. *IEEE TPAMI*, 45(7):9055–9071, 2022. [1](#), [2](#)
- [30] Jianqiang Wang, Dandan Ding, Hao Chen, and Zhan Ma. Dynamic point cloud geometry compression using multiscale inter conditional coding. *arXiv preprint arXiv:2301.12165*, 2023. [1](#)
- [31] Jianqiang Wang, Ruixiang Xue, Jiaxin Li, Dandan Ding, Yi Lin, and Zhan Ma. A versatile point cloud compressor using universal multiscale conditional coding–part i: Geometry. *IEEE transactions on pattern analysis and machine intelligence*, 2024. [1](#), [2](#), [5](#), [6](#)
- [32] Jianqiang Wang, Ruixiang Xue, Jiaxin Li, Dandan Ding, Yi Lin, and Zhan Ma. A versatile point cloud compressor using universal multiscale conditional coding–part i: Geometry. *IEEE transactions on pattern analysis and machine intelligence*, 2024. [1](#), [2](#), [6](#)
- [33] Shuting Xia, Tingyu Fan, Yiling Xu, Jenq-Neng Hwang, and Zhu Li. Learning dynamic point cloud compression via hierarchical inter-frame block matching. In *Proceedings of the 31st ACM International Conference on Multimedia*, pages 7993–8003, 2023. [2](#)
- [34] Junteng Zhang, Tong Chen, Dandan Ding, and Zhan Ma. Yoga: Yet another geometry-based point cloud compressor. In *Proceedings of the 31st ACM International Conference on Multimedia*, pages 9070–9081, 2023. [1](#), [2](#)
- [35] Wenjie Zhu, Zhan Ma, Yiling Xu, Li Li, and Zhu Li. View-dependent dynamic point cloud compression. *IEEE Transactions on Circuits and Systems for Video Technology*, 31(2):765–781, 2020. [2](#)